

HIGH POWER OPERATION AND BEAM INSTRUMENTATIONS IN J-PARC SYNCHROTRONS*

T. Toyama*, J-PARC/KEK, Tokai, Naka, Ibaraki 319-1195, Japan

Abstract

Beam monitors developed and utilized at the MR and RCS of J-PARC are presented with emphasis on their special characteristics for a high intensity proton accelerator. Achieved beam characteristics and approach to improve beam intensity is described in connection with the beam monitors. Usage of a transverse RF field to improve the duty factor of the slow extracted beam is also presented.

INTRODUCTION

Two proton synchrotrons are cascaded after the LINAC in J-PARC [1, 2]. The layout of the synchrotrons and beam transport lines is shown in Fig.1. The first synchrotron is a rapid cycling synchrotron, RCS, which receives two proton-bunches with H⁻ charge exchange injection from the LINAC, 181 MeV at present and being upgraded to 400 MeV in this year [3], and accelerates them up to 3 GeV in 25 Hz. The typical number of accelerated particles is $\sim 2.6 \times 10^{13}$ protons/pulse. The operating point is near $v_x = 6.45$, $v_y = 6.42$ [4]. The next one is the MR. It receives two bunches from the RCS four times per one MR cycle, typically 2.48 s for the fast beam extraction (FX) and 6 s for the slow beam extraction (SX). The beams are accelerated up to 30 GeV. The typical number of accelerated particles is 1.2×10^{14} ppp for FX and 3.0×10^{13} ppp for SX. The operating point is near $v_x = 22.40$, $v_y = 20.75$ for FX and $v_x = 22.30 \rightarrow 22.335$, $v_y = 20.78$ for SX [5].

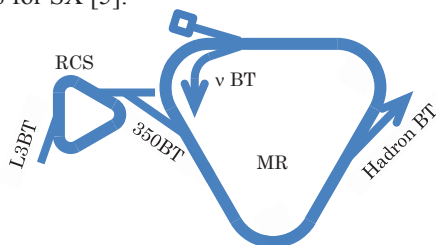


Figure 1: Layout of the RCS, MR and beam transport lines, L3BT, 350BT, Hadron BT and v BT.

OPERATIONAL ASPECT OF THE INSTRUMENTS

To meet the requirements from the high intensity beam operation, three bunch shape monitors (BSMs) at the LINAC [6], a vibration wire monitor (VWM) at the L3BT [7], an ionization profile monitor (IPM) in the RCS [8], an OTR/fluorescent monitor at the 350BT [9] and two exciters in the MR were added by April 2013. Using these beam monitors on top of the present beam monitors [10], the machine study and operation are progressing.

*takeshi.toyama@kek.jp

Identification and Manipulation of Small Beam Losses

Beam loss is a potential limit of the beam intensity and power in J-PARC accelerators. As a rule of thumb the beam losses of 1 W/m in the RCS and 0.5 W/m in the MR are the upper limits except at the collimators and SX areas [1]. The practical and precise investigation of comparison between the beam loss and residual radiation has been performed to keep the activation level smaller than the allowable level, e.g. < 1 mSv/h at one foot distance. Several trials have been performed to identify and mitigate beam losses.

One example is the beam loss measurement during an RCS high beam intensity trial up to 530kW [4]. The beam loss was localized at the collimator within the measurement resolution. The temporal evolution of the beam loss is recorded with the DCCT and SCT (“slow” current transformer) waveform. The beam intensities are normalized by the injected current that is measured with the SCT76 at L3BT (Fig.2). Beam losses are measured by the BLM with a scintillator and a photomultiplier installed by the collimator (Fig.3). The beam losses are plotted with variable intensities up to 539kW. The beam losses are normalized such that the integrated loss at 539 kW equals to 2 %. The temporal evolutions of the losses were used for optimization of the machine parameters by comparing to the simulation using a ring model [4].

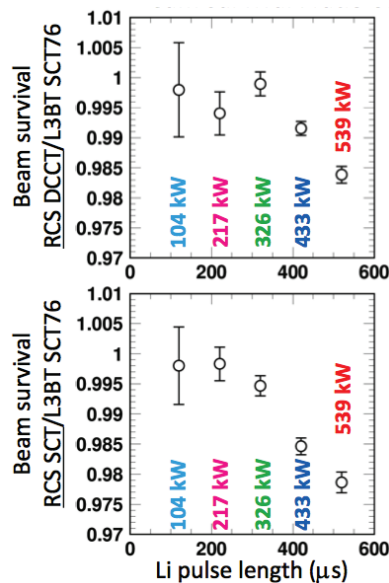


Figure 2: Intensity dependence of the beam loss with variable intensities up to 539kW. The intensities are normalized by the current SCT76 at L3BT.

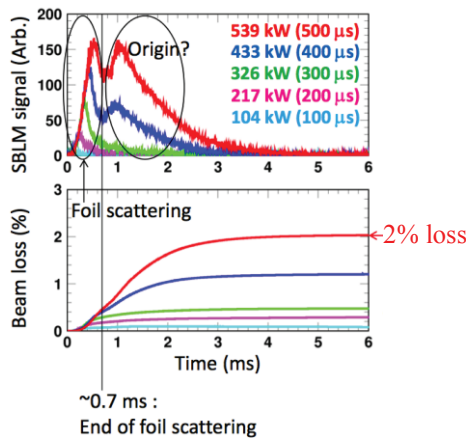


Figure 3: Beam losses with variable intensities up to 539kW. The beam losses are normalized such that the integrated loss at 539 kW equals to 2%.

Another example is the trial to measure the beam tail and halo with the BLMs at the 350BT collimator. The BLMs are composed of 43m-long AICs (air-ionization chambers) and 1m-long AICs calibrated with the DCCT at RCS [11]. The first collimator pair out of 6 pairs was moved vertically. The loss signal at each jaw position was converted to the beam loss (Fig. 4). The beam losses were localized again. The vertical positions were converted to normalized coordinates using Twiss parameters, because the longitudinal positions of the jaws are different. Finally the beam profile with a tail was obtained as shown in Figure 5.

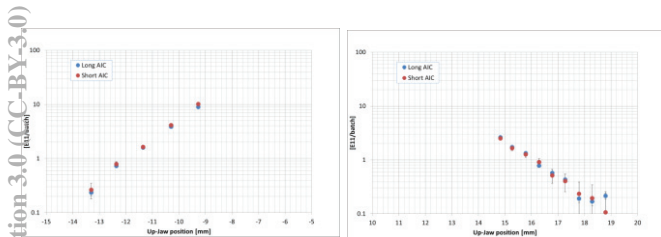


Figure 4: Beam tail measurement at the collimator of the 350BT. The vertical jaws at the first collimator pair were moved. The loss were measured with calibrated BLMs.

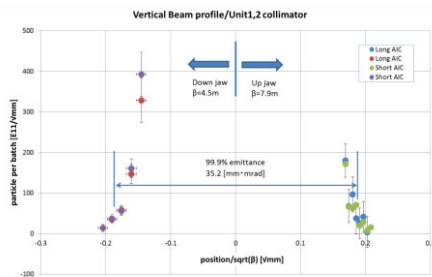
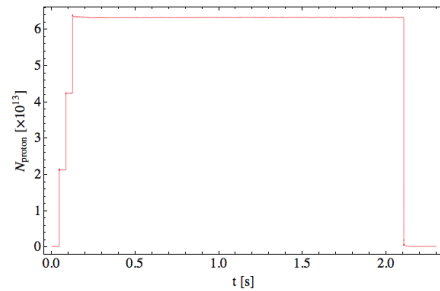
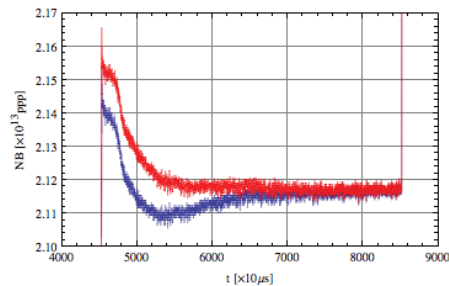


Figure 5: Beam tail measurement at the collimator of the 350BT. The positions are converted to normalized coordinates.

The beam losses are not always localized as in the above examples. And not all BLMs are calibrated yet. In these cases the current monitor is important and need to be accurate enough, i.e. $\Delta I/I < 0.1\%$, to examine $\sim 100W$ loss at an injection period. The DCCT in the MR had a small erroneous response as a blue curve in Fig.6 (b). This response has been corrected using the step response at the FX timing at the end. The IIR filter to cancel the erroneous response was once obtained and applied for correction (Fig. 6 (b) red curve) [12].



(a)



(b)

Figure 6: The DCCT erroneous response and its correction using the step response at the FX timing at the end. (a) The temporal evolution of the MR beam intensity measured with the DCCT. (b) The blue (red) curve is before (after) correction with the injection part zoomed.

Using the constant IIR coefficients caused slow drift of the corrected intensity value at an order of an hour. The reason is under investigation. The intensity correction is performed using simplified correction in shot-by-shot.

Beam Based BPM Calibrations

The BPMs position data provide a wide range of important optics parameters such as betatron function, betatron tune, chromaticity, betatron phase, and dispersion function [4, 5]. Those parameters are the basis of machine modelling and applied for the orbit optimizing process as mentioned above. Accuracy of those parameters depends on the BPMs accuracy. Thus it is worth executing the BPM calibration.

Two kinds of calibrations have been performed, so called “beam based alignment (BBA)” [13] and beam based gain calibration [14, 15].

Ordinary BBA uses one BPM for one quadrupole magnet to calibrate the BPM offset relative to the neighbouring quadrupole magnetic center. However RCS

quadrupoles can be only excited in a group where quadrupoles are serially connected within a “family”. Therefore the calibration method using multiple BPMs with multiple quadrupoles in a family was developed and successfully applied to the RCS BPMs [13]. This method was also applied for a few BPMs in the MR and compared with the results of the ordinary one by one method. Those agreed with each other within expected errors.

The beam based gain calibrations have been successfully applied to the KEKB BPMs [14]. The KEKB BPMs are composed of four small buttons of 12 mm in diameter, located 90 degree apart from each other, on the plane perpendicular to the beam axis (Fig.7 (a)). The BPMs in the J-PARC rings have electrodes with diagonal-cut (Fig.7 (b)). The calibration method was modified to fit this configuration and tested with beams. The result appears promising [15].

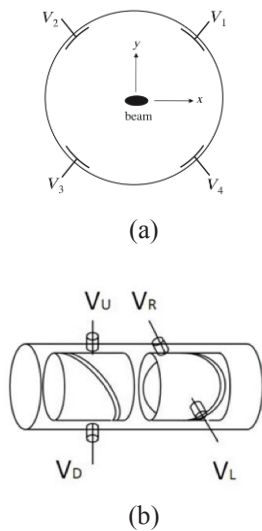


Figure 7: Structure of the BPM: (a) KEKB MR, (b) J-PARC RCS and MR.

Profile, Tail and Halo Measurements

Other than beam profile and tail measurement with the BLMs and collimators mentioned above, measurements with the VWM, OTR/fluorescent monitor, IPM and flying wires have been progressing.

The VWM was installed at the L3BT and has been utilized for tail and halo measurements [7].

The OTR/fluorescent monitor was installed at 350BT. The wide opening angle of the OTR at the beam energy of 3 GeV ($\gamma=4.2$) and a large beam size lead to the wide aperture relay optical system based on Offner system [9]. The three kind of targets, Ti foil 10 μ m thick, Al foil 100 μ m thick with a hole 50 mm diameter, and fluorescent screen: Chromium doped Al_2O_3 500 μ m thick, are shown from left to right in Fig.8. The beam profile was successfully measured at the highest intensity of the 350BT (Fig.9). The tail and halo measurement has just started making use of large light yield of Chromium doped Al_2O_3 .



Figure 8: OTR/fluorescent screen at 350BT. Ti foil 10 μ m thick, Al foil 100 μ m thick with a 50 mm diameter hole, and fluorescent screen: Chromium doped Al_2O_3 500 μ m thick, are shown from left to right.

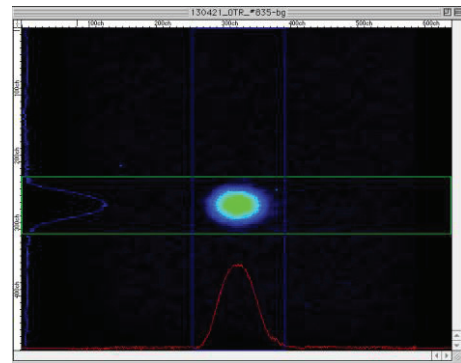


Figure 9: Image of the proton beams, 4.2×10^{13} p / 2 bunches, obtained during the high intensity beam trial.

There are two flying wires in the MR [16]. One for the horizontal, another is for the vertical plane measurement. The wire is made of a carbon fiber of 7 μ m in diameter. Scanning speed is 5 m/s at maximum. The measured profile at the highest beam intensity ever successfully scanned, 1.33×10^{13} ppb, is shown in Fig.10. With two bunches of the beam of intensity 2.2×10^{13} p/bunch the wire was broken. The reason and remedies are under investigation.

Three IPMs (ionization profile monitors) are in the RCS [8] and three IPMs are in the MR [17]. The IPMs in the MR are operated in an ion collection mode, and have no magnets to confine electrons along the magnetic field lines. The profile measurements are performed to optimize an injection matching where the relative size gives useful information. The example is shown in Fig. 11.

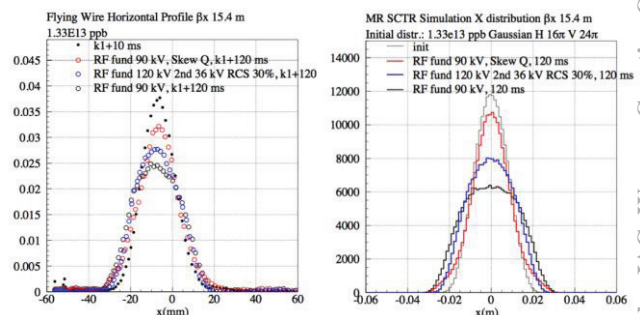


Figure 10: Horizontal beam profile at the beam intensity 1.33×10^{13} ppb. The left plots are measured and the right plots are simulation results.

An effort to obtain the correct size is under way. Three IPMs with magnets in the RCS were improved in electric field uniformity. The calibration with beams shows the position sensitivities normalized by the expected values as 0.934 and 1.116 for ion and electron collection mode, respectively [8].

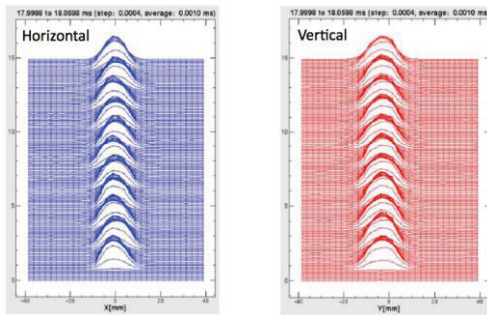


Figure 11: Horizontal (blue) and vertical (red) profiles at the MR. Temporal evolution of one bunch are shown during 11 turns after injection.

Stripline Kickers as "Exciters"

Two stripline kickers were installed in the MR at the beginning of commissioning, one for the horizontal and another for the vertical plane [10]. The length is ~1.5 m, the shunt impedance is ~29 kΩ at the revolution frequency, and the first notch of the shunt impedance is at ~100 MHz. These kickers have been used as exciters for horizontal and vertical tune measurements. An additional circuit for transverse bunch-by-bunch feedback was implemented and used [18]. Intra-bunch feedback study is also under way using these kickers [19]. The horizontal exciter was used for "stochastic slow extraction [20]" with transverse RF during slow beam extraction, which utilises the third-integer resonance, $3\nu_x=67$ [21]. The RF power at 50 M – 100 MHz is, however, too low to meet the requirements of physics groups. Therefore two shorter exciters with a length of ~0.75 m were installed in FY2011 and FY2012. The shunt impedance is ~7 kΩ at the revolution frequency, and the first notch of the shunt impedance is at ~200 MHz. The setup for the SX mode is shown in Fig. 12. In the FX mode they are separated and one kicker is used for B×B feedback and the other is short-circuited at all four ports.

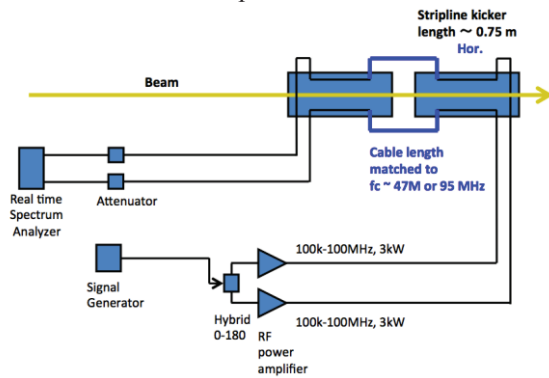


Figure 12: Transverse RF system with two 3 kW power amplifiers and the exciter at #159 in MR.

The beam spill quality is characterized with the duty factor and the extraction efficiency. The duty factor is defined as

$$D = \left[\int_{T_1}^{T_2} I(t) dt \right]^2 / (T_2 - T_1) \int_{T_1}^{T_2} I(t)^2 dt, \quad (1)$$

where $I(t)$, T_1 , and T_2 are the spill current, start- and stop-timing of evaluation, respectively. D takes the maximum value, 1, when $I(t)$ is a constant in time. The extraction efficiency is measured with calibrated BLMs.

The duty factor of the MR SX suffers from large betatron tune ripples due to the quadrupole and dipole magnets current ripples. Among several remedies the stochastic slow extraction with the transverse RF has been successfully implemented. It was originally proposed by S. van der Meer [20] where longitudinal diffusion was considered. The longitudinal diffusion cannot produce horizontal diffusion in the MR because the chromaticity is almost zero during SX. Therefore a transverse RF system for the horizontal direction is adopted.

The signal is a narrowband noise with minimized amplitude variation of bandwidth 0 – 200 Hz and the carrier frequencies of 47 M or 95 MHz depending on the request from the experimental users [22, 23, 24]. The baseband signal (Fig. 13) is upconverted using the IQ modulation with the RF vector signal generator [25].

During the power test of the exciter, the vacuum pressure rise occurred due to multipacting. Three pairs of electrodes: made of type SUS316L stainless steel, SUS316L with TiN coating and SUS316L with DLC (diamond like carbon) coating were prepared to examine secondary electron yield reduction. The thickness of the coating was ~1 μm. Each electrode pair was set in the exciter and we evaluated the pressure rise as a function of the RF- frequency and voltage. The DLC coated electrode pair which suppressed the pressure-rise the most in this experiment, was adopted for the exciter [26]. The solenoid coils were wound outside of the exciters and produce the fields of ~30 G to make multipacting suppression perfect.

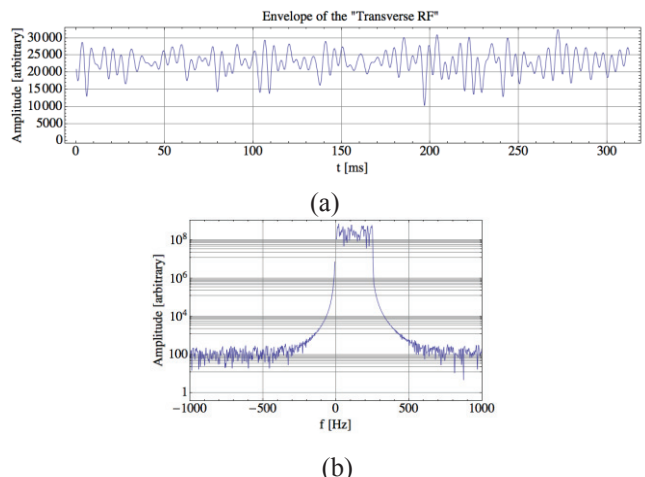


Figure 13: Narrow band noise signal (a) in the time domain and (b) in the frequency domain.

Copyright © 2013 by JACoW — cc Creative Commons Attribution 3.0 (CC-BY-3.0)

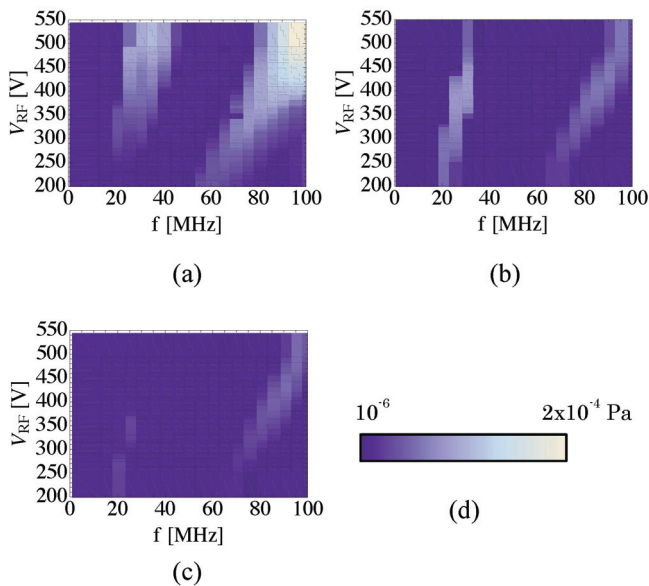


Figure 14: Vacuum pressure rise due to multipacting in the exciter caused by RF. Electrodes are (a) SUS316L, (b) TiN-coated SUS316L (c) DLC-coated SUS316L (d) the color scale of the measured pressure (log scale).

With the assistance of the transverse RF system, the spill duty factor has been improved from ~17 % to more than 40 % and utilized in the operation for experimental users. The temporal evolution of the signal spectrum shown in Fig. 15 (a) is one of the patterns that resulted in a good duty factor. Keeping the bandwidth at 200 Hz, the carrier frequency was shifted by 600 Hz at the middle of the extraction period. The temporal evolution of the beam spill and duty factor are shown in Fig.15 (b) and (c). Another carrier frequency of ~47MHz is also used with a duty factor of more than 40 % (Fig.16).

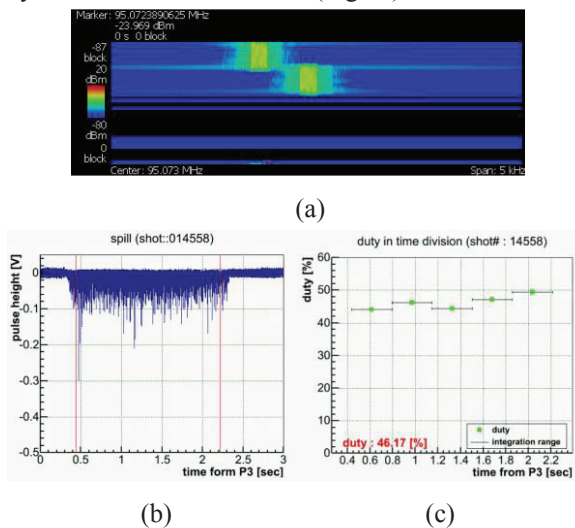


Figure 15: Slow beam extraction with improved duty using the transverse RF. The carrier frequency is ~95MHz in this case. The duty factor was ~46% and the extraction efficiency was 99.5% in this case.

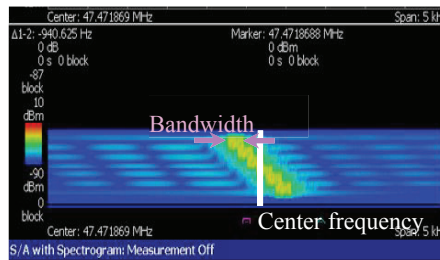


Figure 16: Frequency spectrum of the transverse RF of another pattern, carrier frequency, ~47 MHz and bandwidth of 200 Hz.

SUMMARY

The high intensity proton beam of 300 kW at the RCS and 230 kW (15 kW) for FX (SX) at the MR have been supplied for the MLF, neutrino and hadron users. The full use of the beam monitors has been achieved with beam based calibrations: BLMs calibration by the DCCT and SCT, DCCT response calibration, BPM offset calibration (BBA) and BPM gain calibration. Beam profile, tail and halo measurements are progressing with newly installed devices. Using the transverse RF system the spill duty factor of slow beam extraction has been improved more than twice.

REFERENCES

- [1] Y. Yamazaki ed., KEK Report 2002-13, JAERI-Tech 2003-044 (2003).
- [2] K. Hasegawa et al., IPAC2013, THPW0031, (2013).
- [3] H. Oguri, IPAC2013, WEYB101, (2013).
- [4] H. Hotchi et al., presented by S. Machida, the talk at 14:30, Tue. 16 Apr. 2013, SPACE CHARGE 2013, <http://indico.cern.ch/conferenceDisplay.py?confId=221441>.
- [5] Koseki et al., Prog. Theor. Exp. Phys. (2012) 02B004.
- [6] A. Miura et al., IPAC2013, MOPME027, (2013).
- [7] K. Okabe et al., IPAC2013, MOPME028, (2013).
- [8] H. Harada et al., IPAC2013, MOPME021, (2013).
- [9] M. Tejima et al., IBIC2012, MOPB67, (2012).
- [10] T. Toyama et al., DIPAC2011, TUOA01, p.275 (2011).
- [11] K. Satou, IPAC2012, MOPPR028, p.837 (2012).
- [12] T. Toyama et al., Proc. of the 8th Ann. Meet. of Part. Acc. Soc. of Japan, p.465 (in Japanese).
- [13] N. Hayashi, Nucl. Instrum. Methods Phys. Res., Sect. A 677 (2012) 94.
- [14] M. Arinaga, M. Tejima et al., Prog. Theor. Exp. Phys. (2013) 03A007.
- [15] M. Tejima et al., DIPAC2011, MOPD22, p.92, (2011).
- [16] S. Igarashi, IPAC2011, TUPC098, p.1239, (2011).
- [17] K. Satou et al., HB2010, WEO1C05, p. 506 (2010).
- [18] Kurimoto, DIPAC2011, TUPD74, p.482 (2011).
- [19] O. Konstantinova et al., IPAC2013, TUPWA009, (2013).
- [20] S. van der Meer, CERN/PS/AA 78-6 (1978).
- [21] M. Tomizawa et al., IPAC2012, MOPPD051, p.481 (2012).
- [22] A. Schnase et al., IPAC2010, TUPEA051, p.1446, (2010).
- [23] A. Schnase et al., Proc. of the 8th Ann. Meet. of Part. Acc. Soc. of Japan (2011) p.338.
- [24] A. Schnase et al., LLRF2011, the poster at 14:46, Wed. 19, Oct. 2011, <http://llrf2011.desy.de/e126815/>.
- [25] Agilent technology, N5172B, <http://www.home.agilent.com>
- [26] M. Okada et al., in preparation.